High-power single-stage single-crystal Yb:YAG fiber amplifier for radially polarized ultrashort laser pulses

Michael Eckerle, Frieder Beirow, Tom Dietrich, Frederik Schaal, Christof Pruss, Wolfgang Osten, Nicolas Aubry, Matthieu Perrier, Julien Didierjean, Xavier Delen, et al.

High-power single-stage single-crystal Yb:YAG fiber amplifier for radially polarized ultrashort laser pulses

Michael Eckerle[1,2], Frieder Beirow[1], Tom Dietrich[1], Frederik Schaal[3], Christof Pruss[3], Wolfgang Osten[3], Nicolas Aubry[4], Matthieu Perrier[4], Julien Didierjean[4], Xavier Délen[5], François Balembois[5], Patrick Georges[5], Marwan Abdou Ahmed[1], Thomas Graf[1]

Abstract We report on a single-stage high-power amplification of a radially polarized mode-locked laser beam in a single-crystal fiber (SCF) amplifier. The seed beam was amplified by a factor of 5.0 to an average output power of 66.3 W. The pulse duration of the amplified pulses was measured to be 909 fs at a repetition rate of 40.7 MHz, corresponding to a pulse energy of 1.63 μJ and a resulting pulse peak power of 1.58 MW. The output beam showed a very high quality of the doughnut-shaped intensity distribution and furthermore a high radial polarization purity.

1 Introduction

During the past decades, the LG01* mode with its doughnut-shaped intensity distribution and the axially symmetric (radial or azimuthal) polarization state has attracted an increasing interest due to its unique properties. The non-isotropic polarization orientation and the possibility to sharply focus such a beam [1] makes it a versatile tool for various applications [2] such as plasmon excitation, optical trapping and laser material processing. In the field of cutting thick metal sheets with a radially polarized laser the benefits were outlined theoretically in 1999 by Niziev et al. [3]. In 2007 it was demonstrated by Meier et al. that the drilling speed of holes in mild steel with a Q-switched nanosecond laser can be increased by a factor of 1.5–4 by using azimuthally polarized laser radiation instead of linear or circular polarization [4]. Furthermore, it was experimentally shown that picosecond lasers with such polarization states are promising tools for the fabrication of micro holes [5].

Axially symmetric polarized laser radiation can be either generated intra- or extra-cavity. While the latter was realized at high average powers in the multi kW range, e.g. by means of segmented half-wave plates and a multimode input beam [5], the former has been demonstrated with different approaches such as customized fibers [6], a triple-axicon retroreflector unit [7], the so-called Giant Reflection to Zero Order (GIRO) mirror [8] or grating mirrors [9, 10]. Up to now the listed intra-cavity approaches were only demonstrated in continuous wave (CW) operation. To generate pulsed beams with axially-symmetric polarization states at high average power so far only the aforementioned segmented half-wave plates were used to transform an incident linearly polarized fundamental-mode laser beam into a radially or azimuthally polarized LG01* mode. 85 W of average output power and radially polarized pulses as short as 750 fs were, for instance, achieved by means of three cascaded single-crystal fiber (SCF) amplifier stages starting from a linearly polarized seed beam with an average power of 1.5 W [11]. The polarization conversion was implemented between the second and the third amplification stage. An even higher output power was demonstrated

[1] Institut für Strahlwerkzeuge (IFSW), University of Stuttgart, Pfaffenwaldring 43, 70569 Stuttgart, Germany

[2] Graduate School of Excellence advanced Manufacturing Engineering (GSaME), University of Stuttgart, Nobelstrasse 12, 70569 Stuttgart, Germany

[3] Institut für Technische Optik (ITO), University of Stuttgart, Pfaffenwaldring 9, 70569 Stuttgart, Germany

[4] Fibercryst SAS, Parc d'activité Wilson Bât A1, 31 Rue Wilson, 69150 Decines Charpieu, France

[5] Laboratoire Charles Fabry, Institut d'Optique Graduate School, CNRS, Université Paris-Saclay, 91127 Palaiseau Cedex, France

by amplifying a mode-locked and radially polarized beam with 115 W of seed power to 635 W in a thin-disk multipass amplifier [12]. The seed laser delivered pulses with a duration of 6.5 ps and its fundamental-mode output beam was transformed into a radially polarized doughnut beam again by using a segmented half-wave plate. However, there are several disadvantages when using such a device. The transformation efficiency is limited to about 90% because of scattering and diffraction at the interfaces between the different segments. Furthermore, the scattered and diffracted light deteriorates the beam quality which usually requires further lossy beam cleaning steps. Recently, we reported on the first mode-locked thin-disk oscillator directly delivering radially polarized femtosecond pulses at 13.3 W of average output power and a close to perfect doughnut-shaped beam profile [13] which avoids the need for extra-cavity polarization conversion. This is a promising seed source for further amplification in an Yb:YAG SCF amplifier. In this paper, we, therefore, present the investigations on the application of a high-power single-stage SCF amplifier to increase the power of a radially polarized mode-locked laser beam in order to improve the quality and polarization purity of the doughnut-shaped output beam and to simplify the overall complexity as compared to [11].

2 Seed laser

A modified version of the radially polarized mode-locked laser presented in [13] was used as the seed laser. Mode-locked operation of the laser was obtained by using a semiconductor saturable absorber mirror as a cavity end mirror. The radial polarization was achieved by the use of a so-called grating-waveguide output coupler (GWOC). This component consists of alternating corrugated layers of TaO_5 and SiO_2 on a micro-structured fused silica substrate with an anti-reflection coating on the backside. Such a device is operated at normal incidence and exhibits different reflectivities for beams with radial and azimuthal polarization which results from coupling of the light of one polarization to leaky modes within the multi-layers. A more detailed explanation of the design and the underlying physical effects can be found in [14]. Figure 1 shows the measured wavelength-dependent reflectivity of the GWOC used in the present work. It was characterized with a customized reflectivity measurement setup for radial and azimuthal polarization. The average output power of the seed laser was 13.3 W. It delivered pulses with a duration of 800 fs at a repetition rate of 40.7 MHz, corresponding to a pulse energy of 0.33 µJ and a resulting pulse peak power of 0.36 MW. The M^2-value was measured to be 2.0 which is consistent with the value expected for a LG01* mode. Figure 2 shows the far field intensity distribution of the seed

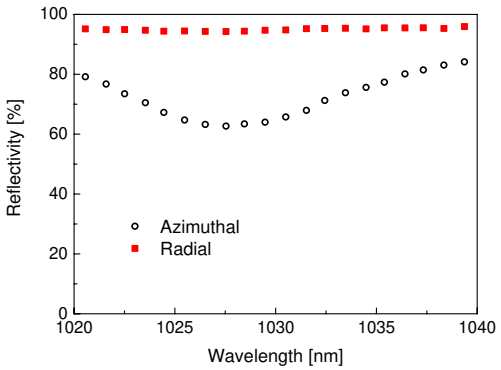

Fig. 1 Reflectivity of the grating-waveguide output coupler (GWOC) measured with a customized reflectivity measurement setup for radial and azimuthal polarizations

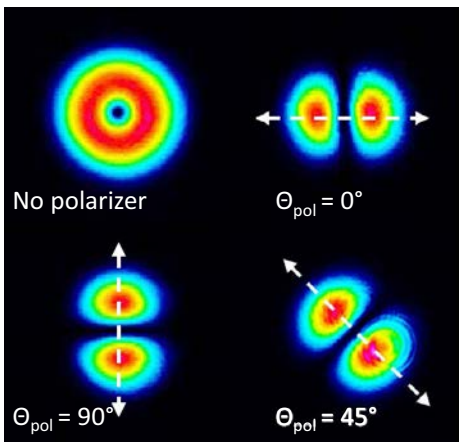

Fig. 2 Far field image of the seed beam (*top left*) transmitted through a linear polarizer with horizontal (*top right*), vertical (*bottom left*) and 45° (*bottom right*) orientation (as indicated by the *white arrows*)

beam as well as the qualitative polarization analysis of the beam recorded with a CCD camera behind a polarizer at different orientations of the polarizer's transmission axis. The white arrows indicate the orientation of the polarization that is transmitted by the polarizer. The well-separated lobes reveal the high purity of radial polarization. This was further confirmed by the measured degree of radial polarization (DORP) of 96.8 ± 1 % which was measured with a camera-based 2D-polarimeter [15][16].

3 Amplification stage

The output beam of the seed laser was amplified in a single-stage Yb:YAG SCF amplifier according to the setup sketched in Fig. 3. The SCF had a diameter of 1 mm and a length of 40 mm. The doping concentration of the

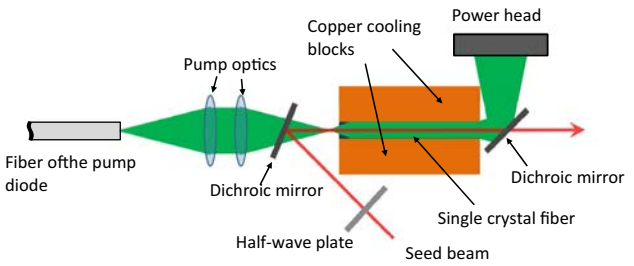

Fig. 3 Schematic of the SCF amplifier setup

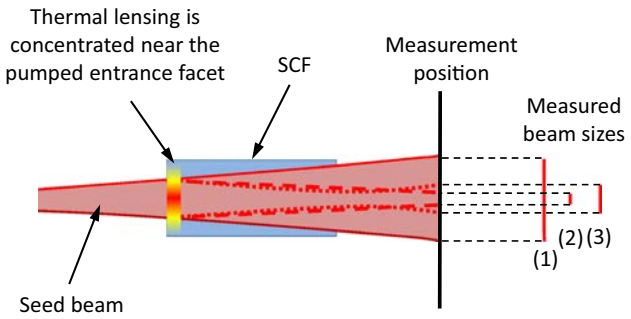

Fig. 4 Principle approach used to test the lensing effect of the SCF. *(1)*, *(2)* and *(3)* indicate the expected relative beam sizes measured at low, medium and high pump power, respectively

Yb:YAG SCF was 0.5 at.%. The chosen doping level was lower than the standard doping of 1 at.% [17], in order to reduce the thermal effects expected from the high pump power absorbed in the SCF. The crystal was mounted between two water-cooled copper blocks to achieve sufficient heat removal. The amplifier was pumped using a fiber-coupled pump diode. The central wavelength of the radiation emitted from the diode was 969 nm which corresponds to the wavelength of the zero-phonon pumping transition of Yb:YAG. This leads to a reduction of the thermal load in the laser crystal as compared to pumping at a wavelength of 940 nm [18]. The fiber of the pump diode had a core diameter of 600 µm and a numerical aperture of 0.22. The pump beam was collimated using an aspherical lens with a focal length of 80 mm. A second aspherical lens with a focal length of 80 mm was used to focus the pump approximately 2 mm in front of the anti-reflection (AR) coated entrance facet of the SCF. The seed laser and the pump light were superimposed coaxially by means of a dichroic mirror which was AR-coated for the pump wavelength and highly reflective for the wavelength of the seed laser (1030 nm) at an angle of incidence of 22.5°. As the pump light was not completely absorbed during one pass in the SCF, a second dichroic mirror was used to separate the seed and the residual pump light. The latter was subsequently directed to a beam dump. While the pump light of the SCF is guided by total internal reflection at the SCF walls the seed beam is supposed to pass the amplifier without being reflected at the walls to maintain the M^2-value [19]. The seed beam was, therefore, focussed to a beam waist diameter of 250 µm at a distance of 28 mm in front of the amplifier, which resulted in a slightly divergent beam with a diameter of approximately 500 µm at the entrance facet of the SCF. This way excessive clipping of the seed beam at the entrance and the exit facet of the SCF was avoided. The divergence of the seed beam was necessary to prevent focusing of the laser beam inside the SCF since the resulting high fluences would damage the SCF. Generally, for pulsed laser beams such a focus can occur as a result of thermal lensing and Kerr lens self-focusing. However, due to the special intensity distribution of the doughnut mode, Kerr lensing plays only a minor role at the power levels presented in this work. To ensure that a thermally induced focus is not present for the applied power levels a preliminary test was done by measuring the beam size at a distance of approximately 45 cm from the end facet of the SCF as sketched in Fig. 4. Due to the divergence of the seed one expects a comparatively large beam at low pump power levels [see Fig. 4(1)] which first becomes smaller with increasing power due to the combined effects of self-focusing and thermal lensing, wherein the latter primarily takes place in the first few millimeters of the SCF due to the high pump power densities [see Fig. 4(2)]. With further increasing pump powers the lensing gets so strong that the beam is refocussed and the waist position will approach the exit facet of the SCF. This results in an increase of the measured beam diameter as soon as the waist passes the measurement position [see Fig. 4(3)]. The applied pump powers were considered to be uncritical as long as the measured beam diameter after the SCF is not rising with increasing pump power. This was the case for all pump power levels used in the experiments reported in the following. The SCF and the dichroic beam splitter after the amplifier introduced a linear phase shift between horizontal and vertical polarization which amounted to approximately 180°. Thus, it was possible to compensate the phase shift by placing a halfwave-plate into the beam path with the main axis along the vertical polarization axis.

4 Experimental results

Figure 5 shows the average output power of the amplifier and the amount of unabsorbed pump power (measured after the dichroic beam splitter) versus the incident pump power for a seed power of 13.3 W. The maximum average output power was 66.3 W for an incident pump power of 519 W which corresponds to a gain factor of 5.0. Within a duration of half an hour the maximum output power fluctuated

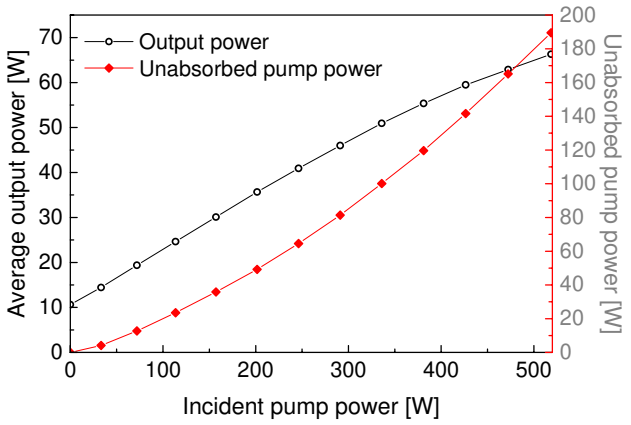

Fig. 5 Average output power and unabsorbed pump power of the SCF vs. incident pump power for an average seed power of 13.3 W

by only ±0.5 W. Figure 6 shows the autocorrelation (AC) traces and the spectra of the seed and the amplified beam. The pulse width increased from 800 to 909 fs as a result of gain narrowing which is visible in the spectral width of the laser radiation that decreased from 1.46 nm before to 1.29 nm after amplification. Thus, the time bandwidth product of the pulses of 0.33 stayed unaffected by the amplification. The pulse energy after amplification was 1.63 µJ and the resulting pulse peak power is 1.58 MW. $Sech^2$-shaped pulses were assumed for the fit function and the calculation of the pulse peak power. In order to assess the beam quality the caustic of the amplified beam was measured behind a lens with a focal length of 70 mm. Figure 7 shows the measured beam diameters as well as the corresponding images of the beam at different positions of the caustic. The beam shows only minor distortions which are the combined result of aberrations due to the thermal lens and the aspherical shape of the saturated gain profile in the SCF. For comparison profiles of the seed beam along a comparable caustic (in terms of beam waist radius, divergence and imaging positions) are shown as well. The M^2-values of the amplified beam were measured to be 2.3 and 2.1 (following ISO 11146) in horizontal and vertical

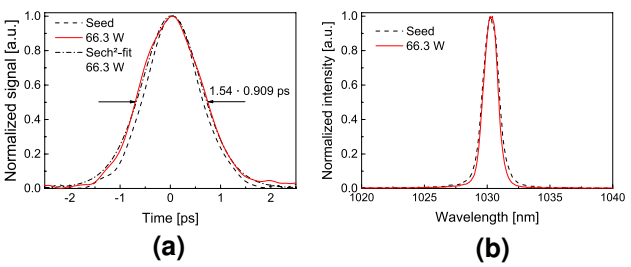

Fig. 6 Autocorrelation traces and spectra of the seed and the amplified beam

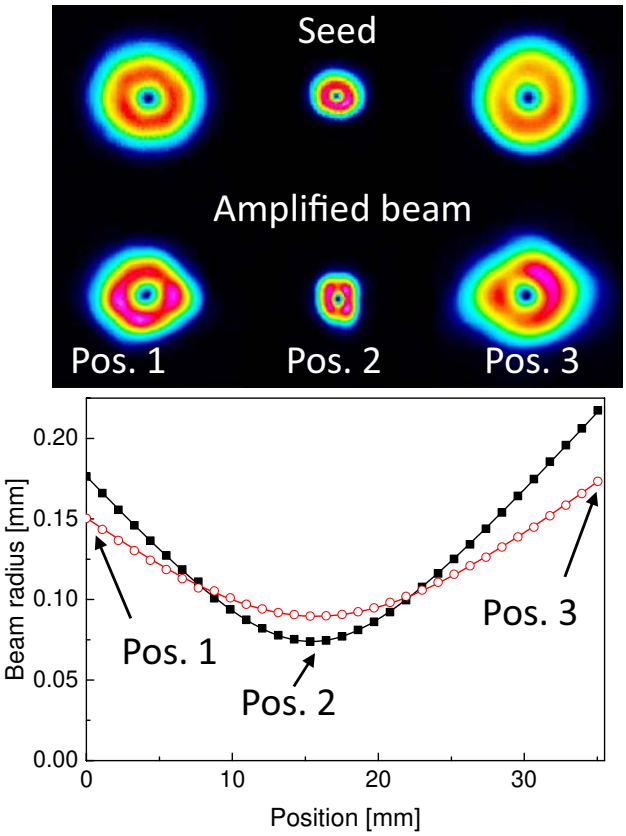

Fig. 7 *Bottom* caustic of the amplified beam measured in the horizontal (*black squares*) and vertical (*red circles*) plane. The *solid lines* represent theoretical fits to the data points. The measured beam radii were determined by the second moment method as defined by ISO 11146. *Top* measured intensity distributions of the amplified beam (*lower row*) at the positions indicated in the graph below and intensity profiles of the seed (*upper row*) along a comparable caustic (in terms of beam waist radius, divergence and imaging positions)

direction, respectively, which is close to the theoretical value of 2.0 expected for an ideal doughnut mode. Figure 8 shows the intensity distribution of the amplified beam and the qualitative polarization analysis of the beam recorded with a CCD camera behind a polarizer at different orientations of its transmission axis. The white arrows again indicate the orientation of the polarization that is transmitted by the polarizer. The images were taken between position 1 and 2 in Fig. 7 at the point where the beam radius is equal in both directions. As can be seen, the intensity distribution at that position is largely axially symmetric and the lobes behind the analyzing polarizer are well separated. To quantify the polarization purity the DORP was measured which amounted to 94±1% for the amplified beam, which is close to the 96.8±1% of the seed beam. The intensity distributions of the seed (a) and the amplified (b) beam are shown in Fig. 9 together with polarization ellipses extracted from the 2D-polarimeter measurement. Without the aforementioned halfwave plate to compensate for the phase shift

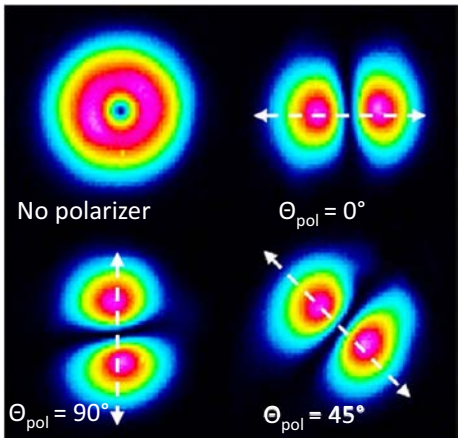

Fig. 8 Far field image of the amplified beam and images of the beam with a polarizer in front of the camera. The *white arrows* indicate the orientation of the polarization that is transmitted through the polarizer

introduced by the SCF and the beam splitter, the polarization distribution would be distorted as shown by (c). The green line in (b) indicates the orientation of the main axis of the half-wave plate that is used for the compensation. From the orientation of the ellipses it is obvious that the compensation worked well and that the phase shift induced by the SCF is homogeneous across the crystal's cross section. The phase front was not measured directly, but the M^2 -value and the DORP indicate that the phase distortions resulting from the amplification were small.

5 Summary and outlook

In summary we have demonstrated the amplification of a radially polarized mode-locked seed laser up to an average output power of 66.3 W at an incident pump power of 519 W by means of a simple single-stage SCF amplifier. At these parameters the gain was 5.0. The pulse duration increased slightly from 800 to 909 fs due to gain narrowing. The homogeneous and axially symmetric intensity and polarization distribution was comparatively well maintained, especially in comparison to experiments with ultrafast lasers at similar average output powers [11]. The promising results encourage further research in which, e.g. the unabsorbed pump power may be reflected back into the SCF to further increase the overall efficiency. Such a

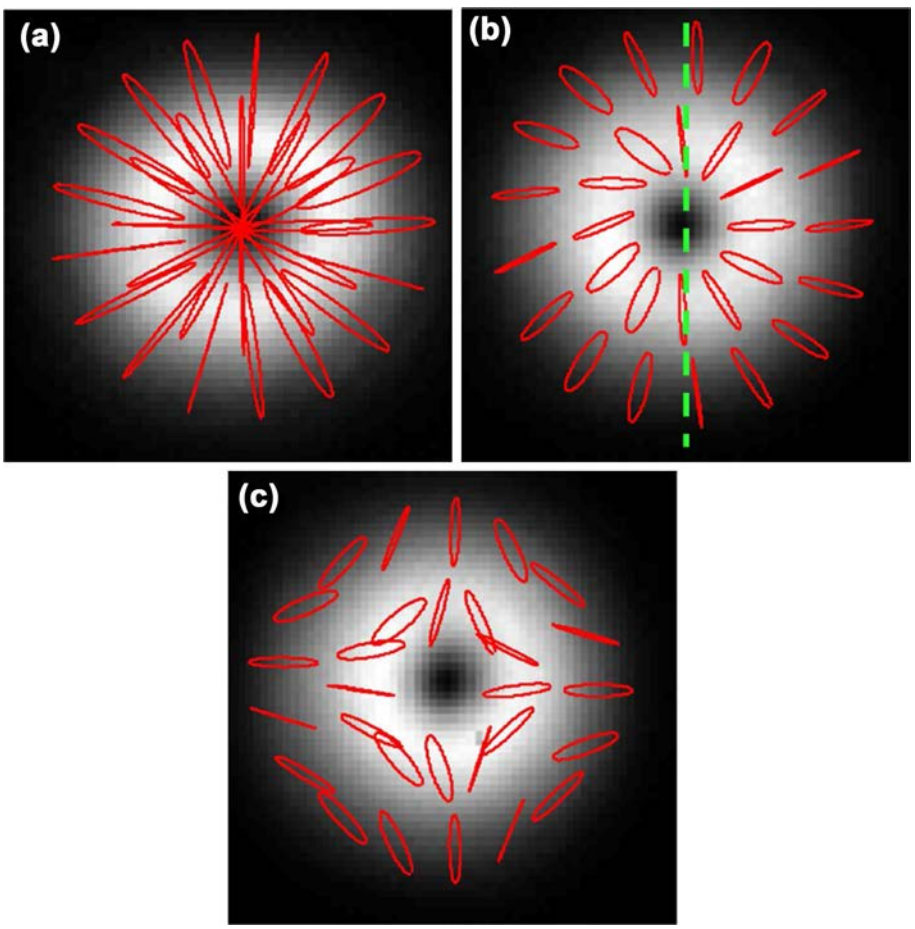

Fig. 9 Far field images of the seed (**a**) and amplified beam, with (**b**) and without (**c**) phase compensation, with the cor-responding polarization ellipses (*red*). The *green line* indicates the orientation of the main axis of the half-wave plate

system can be promising seed for further amplification in a thin-disk multi-pass amplifier [12] and to efficiently reach kW average output powers.

Funding The research leading to these results has received funding from the European Union Seventh Framework Programme FP7/2007-2013 under Grant Agreement no. 619237 and the Deutsche Forschungsgemeinschaft (DFG).

References

1. Q. Zhan, Adv. Opt. Photonics **1**(1), 1 (2009)
2. R. Dorn, S. Quabis, G. Leuchs. Phys. Rev. Lett. **91**(23), 233901 (2003)
3. V.G. Niziev, A.V. Nesterov, J. Phys. D Appl. Phys. **32**(13), 1455–1461 (1999)
4. M. Meier, V. Romano, T. Feurer, Appl. Phys. A **86**(3), 329–334 (2007)
5. R. Weber, A. Michalowski, M.A. Ahmed, V. Onuseit, V. Rominger, M. Kraus, T. Graf, Phys. Proc. **12**, 21–30 (2011)
6. J.M.O. Di Lin, M. Daniel, M. Gecevičius, P.G. Beresna, W.A.Clarkson Kazansky, Opt. Lett. **39**(18), 5359 (2014)
7. M. Endo, Opt. Lett. **33**(15), 1771 (2008)
8. T. Moser, J. Balmer, D. Delbeke, P. Muys, S. Verstuyft, R. Baets, Appl. Opt. **45**(33), 8517 (2006)
9. Thomas Kämpfe, Svetlen Tonchev, Alexandre V. Tishchenko, Deyan Gergov, Olivier Parriaux, Opt. Express **20**(5), 5392 (2012)
10. M.A. Ahmed, J. Schulz, A. Voss, O. Parriaux, J.-C. Pommier, T. Graf, Opt. Lett. **32**(13), 1824 (2007)
11. F. Lesparre, J.T. Gomes, X. Délen, I. Martial, J. Didierjean, W. Pallmann, B. Resan, M. Eckerle, T. Graf, M.A. Ahmed, F. Druon, F. Balembois, P. Georges, Opt. Lett. **40**(11), 2517 (2015)
12. A. Loescher, J.-P. Negel, T. Graf, M.A. Ahmed, Opt. Lett. **40**(24), 5758 (2015)
13. M. Eckerle, T. Dietrich, F. Schaal, C. Pruss, W. Osten, M.A. Ahmed, T. Graf, Opt. Lett. **41**(7), 1680 (2016)
14. M.A. Ahmed, M. Haefner, M. Vogel, C. Pruss, A. Voss, W. Osten, T. Graf, Opt. Express **19**(6), 5093–5104 (2011)
15. T. Liebig, M.A. Ahmed, A. Voss, T. Graf, in SPIE LASE, Photonics West, 2010
16. A. Voss, M.A. Ahmed, T. Graf, Opt. Express **18**(21), 21540–21550 (2010)
17. Fibercryst—High Power Laser Gain Module Taranis for Short Pulses Lasers—Homepage, 09.11.2016. http://fibercryst.com/
18. B. Weichelt, A. Voss, M.A. Ahmed, T. Graf, Opt. Lett. **37**(15), 3045–3047 (2012)
19. D. Sangla, N. Aubry, J. Didierjean, D. Perrodin, F. Balembois, K. Lebbou, A. Brenier, P. Georges, O. Tillement, J.-M. Fourmigué, Appl. Phys. B **94**(2), 203–207 (2009)